

# Interpretable Battery Cycle Life Range Prediction Using Early Degradation Data at Cell Level

Huang Zhang, Yang Su, Faisal Altaf, Torsten Wik, Sebastien Gros

**Abstract**—Battery cycle life prediction using early degradation data has many potential applications throughout the battery product life cycle. Various data-driven methods have been proposed for point prediction of battery cycle life with minimum knowledge of the battery degradation mechanisms. However, management of batteries at end-of-life with lower economic and technical risk requires prediction of cycle life with quantified uncertainty, which is still lacking. The interpretability (i.e., reason for high prediction accuracy) of these advanced data-driven methods is also worthy of investigation. Here, a physics-informed Quantile Regression Forest (QRF) model is introduced to make cycle life range prediction with uncertainty quantified as the length of the prediction interval, in addition to point predictions with high accuracy. The hyperparameters of the QRF model are tuned with a proposed area-based performance evaluation metric so that the coverage probabilities associated with the prediction intervals are calibrated. The interpretability of the final QRF model is explored with two global model-agnostic methods, namely permutation importance and partial dependence plot. The final QRF model facilitates dual-criteria decision-making to select the high-cycle-life charging protocol with consideration of both point predictions and uncertainty associated with the prediction.

**Index Terms**—Lithium-ion battery, cycle life early prediction, quantile regression forest, interpretable machine learning.

This paper has not been presented at any conference or submitted elsewhere.

## I. INTRODUCTION

LITHIUM-ION (Li-ion) batteries have become the main source of energy storage in electric vehicles (EVs), spurred by governmental policies and subsidies with the aim of enhancing energy sustainability and carbon emission reduction [1] [2]. However, Li-ion batteries degrade with time due to both calendar aging and cyclic aging, which leads to a deterioration of their performance [3]. Understanding these aging processes, and providing a reliable cycle life prediction of Li-ion batteries based on early degradation data would enable many new possibilities throughout the battery life. Five examples are given here. Firstly, the total driven distance of an EV can be translated into a number of equivalent full cycles [2]. Reliable cycle life prediction of Li-ion batteries using early degradation data would facilitate automotive companies to adjust their warranty policy quickly for new batches of Li-ion batteries from suppliers, while greatly reducing time and cost of long aging experiments. Warranty and pricing based on prediction of cycle life in the battery second life application as energy storage strongly affect how this market will evolve in the future, and reducing the uncertainty associated with cycle life prediction will reduce the cost of battery deployments [4]. Secondly, accurate and reliable cycle life prediction with high accuracy also facilitates predictive maintenance by reducing the sudden failure rate and the maintenance costs of battery-based applications [5]. Thirdly, prediction of cycle life with high accuracy using early degradation data can reduce the need of full aging characterization test for a large set of cells [6]. Fourthly, an early-prediction model can also be combined with a design parameter optimization algorithm to identify high-cycle-life charging protocols [6]. Lastly, accurate prediction of the battery life with early degradation data is of crucial importance for improving the battery manufacturing processes [7].

Unfortunately, the degradation process of Li-ion batteries is highly nonlinear, and influenced by not only the operating conditions, but also variances due to imperfect manufacturing tolerances. These factors contribute to the complexity of battery cycle life prediction [8]. This complexity and the importance of battery cycle life prediction with high accuracy have made this an intense research area. The prediction methods can be generally divided into two categories - model-based methods and data-driven methods.

The model-based methods can be roughly classified into three categories. In the first one, a physics-based model, such as an electrochemical model (EM), is incorporated into a recursive filter framework, such as the extended Kalman

Corresponding author: Huang Zhang is with the Department of Electromobility, Volvo Group Trucks Technology, 405 08 Gothenburg, Sweden (mobile: +46739022691; email: huang.zhang@volvo.com) and with the Department of Electrical Engineering, Chalmers University of Technology, 412 96 Gothenburg, Sweden (email: huangz@chalmers.se)

Yang Su is with UMR ECOSYS, INRAE - UVSQ, Université Paris-Saclay, 78850 Thiverval-Grignon, France. (email: yang.su@inrae.fr)

Faisal Altaf is with the Department of Electromobility, Volvo Group Trucks Technology, 405 08 Gothenburg, Sweden (email: faisal.altaf@volvo.com)

Torsten Wik is with the Department of Electrical Engineering, Chalmers University of Technology, 412 96 Gothenburg, Sweden (email: torsten.wik@chalmers.se)

Sebastien Gros is with the Department of Engineering Cybernetic, Faculty of Information Technology, NTNU, Gløshaugen, NO-7491 Trondheim, Norway (email: sebastien.gros@ntnu.no)

filter [9] or a particle filter [10], in which internal parameters are updated from measured data. However, poor parameter identifiability, partial differential equations and large matrix computations inevitably limit their applicability in real-time battery management system (BMS). In the second category, empirical models are identified based on cell characterization data from lab experiments. To improve their accuracy in on-board vehicle applications, model parameters can be adapted by the on-board BMS using measurement and state estimation data in a Bayesian filtering framework. This can include a range of Kalman filters [11] and particle filters [12]. The prediction accuracy of empirical models with a recursive filter highly depends on the fitted model. In addition to these two model-filter-based models, a third category of semi-empirical models have also been developed to capture the direct relationship between the operating conditions and the battery state-of-health (SOH), by interpolating and fitting experimental data. The only difference between empirical and semi-empirical model is that the former does not use any physical relation in the model structure whereas the latter uses some level of physical insights in the model formulation. Most semi-empirical models in the literature study the battery calendar aging and cyclic aging separately, and then combine both to make predictions under various operating conditions [13] [14] [15]. Although it is easier to implement semi-empirical models than the model-filter-based methods described, semi-empirical models are open-loop approaches where the model parameters are determined by data fitting.

Data-driven methods for battery cycle life prediction are generally black-box models developed based on machine learning or deep learning approaches. These methods capture the mapping between inputs and desired outputs during training. Data-driven methods can be either non-probabilistic or probabilistic. Non-probabilistic data-driven methods include autoregression (AR) based models [16] [17], artificial neural network (ANN) [18] [19] [20] and support vector machine (SVM) [21] [22]. Despite the high accuracy of these non-probabilistic data-driven methods on cycle life point prediction, they are unfortunately not able to provide any uncertainty level of their predictions. The uncertainty level of predictions can enable a system or a user to make risk-informed decisions [23]. For this reason, probabilistic data-driven methods like Gaussian process regression (GPR) [24] [25] and relevance vector machine (RVM) [26] [27] can be a better choice, as they have the ability to output probability density function (PDF), and predict both the cycle life and the associated confidence interval. However, the development of these probabilistic data-driven methods is still at an early stage. Few existing models are built on battery data under widely varying operating conditions, such as in an EV application since the performance of these data-driven methods is highly dependent on the structure of the selected model and its hyperparameters. Therefore, their robustness and adaptation to real applications are questionable.

As illustrated by Kristen et al. [5], cycle life for battery cells does not follow a normal distribution, which is a required assumption for many probabilistic data-driven methods (e.g., Gaussian process regression models) that provide uncertainty information associated with the predictions. While advanced

data-driven methods offer high prediction accuracy of battery cycle life in spite of minimum knowledge of the battery degradation mechanisms, interpretability of machine learning models is still underexplored in the literature. Extracting relevant battery aging knowledge from a machine learning or deep learning model in terms of underlying relationships either in data or learned by the model can provide valuable insights into battery cycle life prediction. These insights can then be used to guide discoveries of aging mechanisms, improvements of battery manufacturing and development of fast-charging protocols.

This paper tries to tackle the aforementioned problems by proposing a quantile regression forest (QRF) model, which is produced by a machine learning pipeline, for reliable cycle life range prediction of Li-ion battery cells. The prediction intervals are constructed by using a quantile regression method that estimates quantiles of the response variable given values of the input variables [28] [29]. The advantages of the QRF model over other probabilistic models are that asymmetric prediction intervals can be estimated without assuming any specific distribution (e.g., Gaussian distribution) of cycle life, being the output variable. Additionally, the QRF model is a non-parametric method, which means that the number of parameters adapts to the complexity of the training data. To interpret the final QRF model, permutation importance, and partial dependence plot are employed as model-agnostic methods to quantitatively interpret the final QRF model. An area-based performance evaluation metric is then proposed for assessing the performance of the quantile regression models over the whole range of prediction intervals. Point predictions are obtained based on the mean and median of the predicted cycle life delivered by the final QRF model. The accuracy of these point predictions is compared with non-probabilistic parametric Elastic Net regression models, whose prediction performance was successfully demonstrated by Kristen et al. [5]. Lastly, prediction intervals are constructed to assess the reliability of the predictions.

The novelty and contributions are summarized as follows:

- This work proposes the first application of QRF model to quantify the uncertainty in battery cycle life prediction. It is shown that the QRF model not only provides point prediction with high accuracy but also cycle life range prediction with high probability without assuming any specified distribution for cycle life. The performance of the proposed QRF model is demonstrated on the public dataset from Toyota Research Institute, and is benchmarked to the Elastic Net model.
- To interpret the final QRF model for cycle life prediction and reveal the underlying relationships in data learned by the QRF model, permutation importance and partial dependence plot are employed as model-agnostic methods to rank individual feature importance and quantitatively show the marginal effect each feature has on the predicted battery cycle life. Subsequently, an electrochemical interpretation is given to support what has been revealed by these two model-agnostic methods.
- A sensitivity analysis of the QRF model performance using different number of early-cycle data (from the

first 25 cycles to the first 250 cycles) shows that data for the first 100 cycles is a suitable choice for cycle life prediction, considering the trade-off between best possible prediction accuracy and lowest possible number of required cycles.

- In an application of selecting the high-cycle-life charging protocol, the expected battery cycle life of a charging protocol is determined with consideration of both point predictions and uncertainty associated with the prediction. It is demonstrated that the final QRF model facilitates dual-criteria decision-making to select the high-cycle-life charging protocol which maximizes this expected battery cycle life.

## II. MACHINE LEARNING PIPELINE AND PROBLEM FORMULATION

A pipeline-based approach is used to produce the final QRF model. The machine learning pipeline is illustrated in Fig. 1. To start with, predicted cycle life is selected as output variable. Then the battery data is preprocessed and features are extracted. The feature data is split into a training set and a test set. The QRF hyperparameters are tuned to calibrate coverage probabilities associated with prediction intervals. Then the QRF model with optimal hyperparameters is refitted in order to obtain the final model. The resulting final model is used for both point prediction and range prediction. Moreover, the final model is interpreted with two model-agnostic techniques.

### A. Machine learning pipeline

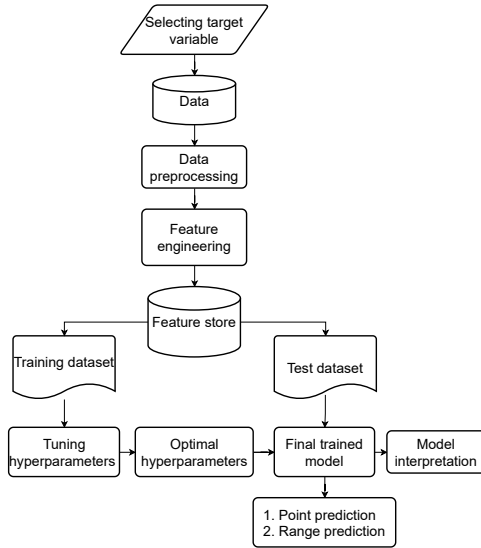


Fig. 1. Machine learning pipeline for cycle life range prediction model.

### B. Feature engineering

Generally, feature engineering can be divided into two categories - automatic feature engineering, such as auto-encoders [30], and restricted Boltzmann machine [31], and manual feature engineering based on domain knowledge [32] [33]. In the present work, battery domain knowledge is adopted in the

feature engineering process. Including the features extracted by Kristen et al. [5], 33 features were extracted from the first 100 cycles data for each battery cell, i.e.,

- minimum, variance, skewness, kurtosis of difference of the discharge voltage curve between cycle 100 and cycle 10 (i.e.,  $\Delta Q_{100-10}(V)$ ) [5];
- amplitude and position shift of highest peak in discharge incremental capacity curve from cycle 10 to cycle 100 (i.e.,  $dQdV_{100-10}$ );
- minimum, variance, skewness, kurtosis of difference of the discharge cell temperature as a function of voltage between cycle 100 and cycle 10 (i.e.,  $\Delta T_{100-10}(V)$ );
- minimum, maximum, mean, variance of discharge cell temperature as a function of voltage at cycle 10 (i.e.,  $T_{10}(V)$ );
- minimum, maximum, mean, variance of discharge cell temperature as a function of voltage at cycle 100 (i.e.,  $T_{100}(V)$ );
- difference of minimum, maximum, mean, variance of discharge cell temperature as a function of voltage between cycle 10 and cycle 100;
- slope of the linear fit to the capacity fade curve from cycle 2 to cycle 100 [5];
- intercept of the linear fit to capacity fade curve from cycle 2 to cycle 100 [5];
- discharge capacity at cycle 2 [5];
- discharge capacity at cycle 100 [5];
- difference between maximum discharge capacity within first 100 cycles and discharge capacity at cycle 2 [5];
- average charge time over first 5 cycles [5];
- minimum internal resistance from cycle 2 to cycle 100 [5];
- maximum internal resistance from cycle 2 to cycle 100;
- internal resistance at cycle 2 [5];
- internal resistance at cycle 100;
- difference of internal resistance between cycle 100 and cycle 2 [5].

At the training and cross validation stages, leave-one-out cross validation (LOO-XVE) method was adopted for tuning the hyperparameters of the QRF model. LOO-XVE is the extreme case of a k-fold cross validation method [34]. The QRF model is trained on all samples in the training set except for one sample, and the validation is made on that sample. LOO-XVE is suitable for small dataset as in the present work in which prediction accuracy also outweighs computational cost at the training and cross validation stages. Optuna [35] is used for tuning the hyperparameters of the QRF model in the cross validation stage. After 250 trials, an optimal set of hyperparameters is obtained. The QRF model is refitted with the whole training set. The final learned model is then interpreted using two global model-agnostic methods. As a fair comparison, the hyperparameters of Elastic Net model is also tuned to optimal after 250 trials via Optuna.

### C. Problem formulation

The battery cycle life prediction problem can be formulated as a regression problem with the goal of learning a

mapping  $f$  from a random input vector (a term we will use interchangeably with features throughout this paper)  $X = (X_1, X_2, \dots, X_p)^T$  in the space  $\mathcal{X} \subseteq \mathbb{R}^p$  to a random output (a term we will use interchangeably with response throughout this paper) variable  $Y$  in the space  $\mathcal{Y} \subseteq \mathbb{R}^+$ ,  $f : \mathcal{X} \rightarrow \mathcal{Y}$ , given a training set  $\mathcal{D} = \{\mathbf{x}_i, y_i\}_{i=1}^N$ , where  $N$  is the number of assumed independent and identically distributed samples in the training set. In the present case,  $\mathbf{x}_i \in \mathcal{X}$  represents  $p$  features extracted from the first 100 cycles, and  $y_i \in \mathcal{Y}$  is the observed battery cycle life.

To learn the mapping function  $f$ , the conditional mean minimizing the expected squared error loss is used,

$$E(Y|X = \mathbf{x}) = \arg \min_{f(\mathbf{x})} E\{(Y - f(\mathbf{x}))^2 | X = \mathbf{x}\}. \quad (1)$$

In practice, the approximation of the conditional mean is achieved by minimization of a squared error type loss function over the training set  $\mathcal{D}$  and the learned regression function is denoted as  $\hat{f}$ .

With parametric methods, the regression function  $f$  is parameterized by a fixed number of parameters. Then the regression problem gets simplified to find the values of these parameters that minimize the loss function over the training set  $\mathcal{D}$ . However, the assumptions made on the function of  $f$  might not always hold and the parameterized function can be very different from the true function [34]. Moreover, parametric regression methods can have a high bias when the number of function parameters is assumed to be low, while a large number of model parameters often lead to a high variance as the regression function may be overfitted on the training set. In contrast, non-parametric methods do not parameterize the regression function  $f$  with a fix number of parameters, the number of parameters grows with the size of the training set instead. Despite the fact that non-parametric methods need a larger dataset to estimate the "best"  $\hat{f}$ , they are more flexible than parametric methods to extract complex patterns in the data without necessarily incurring severe overfitting. One of the most common non-parametric methods is random forest regression.

### III. METHODOLOGY

#### A. Random forest regression

Random forest regression is an ensemble method first introduced by Breiman [36]. Multiple de-correlated decision trees are constructed during the training stage using an algorithm called bootstrap aggregation, or shortly bagging. The essential idea behind bagging is to average the results of many noisy but approximately unbiased models, reduce the variance associated with prediction and leave bias unchanged [34]. Tree-based models can benefit greatly from bagging, since they are capable of capturing complex structures in the data with relatively low bias if grown sufficiently deep, but they are notoriously noisy at the same time. The random forest regression model further improves the variance reduction of bagging by reducing the correlation between the trees. This is achieved by random selection of the input variables from the  $p$  input variables before each split.

There are several advantages of the random forest regression model when it comes to practical implementation. Firstly, trees that grow during the training stage of the random forest model do not require pruning, which leads to light-weight computation. Secondly, there are only two parameters to be tuned during training stage of the random forest model, the number of trees to grow in the forest and the number of random features for each split [34]. This saves considerable efforts when finding the set of parameters that achieve the best performance.

The random forest regression model approximates the conditional mean of  $Y$  given  $X = \mathbf{x}$ ,  $E(Y|X = \mathbf{x})$ , by averaging predictions of  $K$  trees, each growing with an independent and identically distributed (i.i.d.) random parameter vector  $\theta_t$ ,  $t = 1, \dots, K$ . For the  $t$ -th regression tree denoted by  $T(\theta_t)$ , every leaf  $l = 1, \dots, L$  of the regression tree corresponds to a subset of  $\mathcal{X}$ , denoted by  $\mathcal{R}_l \subseteq \mathcal{X}$ . There is one and only one leaf  $l$  such that  $\mathbf{x} \in \mathcal{R}_l$ . This leaf is denoted by  $l(\mathbf{x}, \theta_t)$  in the regression tree  $T(\theta_t)$ .

The prediction of the  $t$ -th regression tree  $T(\theta_t)$  for an input  $X = \mathbf{x}$  is obtained by averaging over the observations  $y_i$  in leaf  $l(\mathbf{x}, \theta_t)$ . Defining the weight  $w_i(\mathbf{x}, \theta_t)$  by:

$$w_i(\mathbf{x}, \theta_t) = \frac{\mathbb{1}_{\{\mathbf{x}_i \in \mathcal{R}_{l(\mathbf{x}, \theta_t)}\}}}{\#\{j : \mathbf{x}_j \in \mathcal{R}_{l(\mathbf{x}, \theta_t)}\}}, \quad i = 1, \dots, N \quad (2)$$

where  $\mathbb{1}_{\{\mathbf{x}_i \in \mathcal{R}_{l(\mathbf{x}, \theta_t)}\}}$  is an indicator function and equal to 1 if  $\mathbf{x}_i \in \mathcal{R}_{l(\mathbf{x}, \theta_t)}$  and otherwise equal to 0. Note that the weights are indexed with respect to all observations in the training set  $\mathcal{D}$  instead of observations in the subsample set on which the  $t$ -th regression tree in the random forest grows. If the  $i$ -th observation is not in the subsample set for the  $t$ -th regression tree, then the weight  $w_i(\mathbf{x}, \theta_t)$  will be 0 for the  $t$ -th regression tree.

The prediction of the  $t$ -th regression tree is a weighted sum of the original observations  $y_i$ ,  $i = 1, \dots, N$ ,

$$\hat{f}_t(\mathbf{x}) = \sum_{i=1}^N w_i(\mathbf{x}, \theta_t) y_i. \quad (3)$$

Let the average of  $w_i(\mathbf{x}, \theta_t)$  over the regression trees grown in the random forest be denoted by  $w_i(\mathbf{x})$ ,

$$w_i(\mathbf{x}) = \frac{1}{K} \sum_{t=1}^K w_i(\mathbf{x}, \theta_t). \quad (4)$$

The prediction of the random forest regression model, i.e., the approximation of the conditional mean of  $Y$  given  $X = \mathbf{x}$  is given by a weighted sum over all observations,

$$\hat{f}(\mathbf{x}) = \sum_{i=1}^N w_i(\mathbf{x}) y_i, \quad (5)$$

where the weights sum up to one.

#### B. Quantile regression forest

The conditional mean only reveals one aspect of the conditional distribution of a response variable  $Y$  and gives very little information about the uncertainty associated with the predicted conditional mean. In our cases, though, we are interested to

find the range of predicted battery cycle life in which the battery will reach its end of life with high probability. This can be achieved with quantile regression, as it gives complete information about the spread of the response variable.

It is shown above that the random forest regression model approximates the conditional mean by a weighted sum over all observations  $y_i$ ,  $i = 1, \dots, N$ . Instead of averaging over observations in every leaf of every tree, one wants to keep all observations in every leaf of every tree in the random forest, which could contribute to the full conditional distribution of the response variable.

Firstly, the conditional cumulative distribution function  $F(y|X = \mathbf{x})$  is defined as the probability of  $Y$  smaller than  $y$  given  $X = \mathbf{x}$ , i.e.,

$$F(y|X = \mathbf{x}) = P(Y \leq y|X = \mathbf{x}). \quad (6)$$

For a continuous conditional cumulative distribution function, as defined above, the  $\alpha$ -quantile  $Q_\alpha(\mathbf{x})$  is defined such that the probability of  $Y$  less than or equal to  $Q_\alpha(\mathbf{x})$  is equal to  $\alpha$  for a given  $X = \mathbf{x}$ ,

$$Q_\alpha(\mathbf{x}) = \arg \min_y \{y : F(y|X = \mathbf{x}) \geq \alpha\}. \quad (7)$$

The conditional cumulative distribution function of the QRF model, is expressed as,

$$F(y|X = \mathbf{x}) = P(Y \leq y|X = \mathbf{x}) = E(\mathbb{1}_{\{Y \leq y\}}|X = \mathbf{x}), \quad (8)$$

where  $\mathbb{1}_{\{Y \leq y\}}$  is an indicator function and equal to 1 if  $Y \leq y$  and otherwise equal to 0. In analogy with the random forest approximation of the conditional mean  $E(Y|X = \mathbf{x})$ , the last expression,  $E(\mathbb{1}_{\{Y \leq y\}}|X = \mathbf{x})$ , can be approximated by the weighted sum over the observations of  $\mathbb{1}_{\{Y \leq y\}}$ . Thus, an empirical conditional probability function  $\hat{F}$ , given  $X = \mathbf{x}$ , can be obtained as,

$$\hat{F}(y|X = \mathbf{x}) = \sum_{i=1}^N w_i(\mathbf{x}) \mathbb{1}_{\{y_i \leq y\}}, \quad (9)$$

where the weights  $w_i(\mathbf{x})$  are the same as defined in (4). The indicator function  $\mathbb{1}_{\{y_i \leq y\}}$  here determines whether the weight will be counted or not, depending on the condition  $y_i \leq y$ .

Finally, the estimated  $\alpha$ -quantile  $\hat{Q}_\alpha(\mathbf{x})$  is obtained by inserting  $\hat{F}(y|X = \mathbf{x})$  in (9) into (7), i.e.,

$$\hat{Q}_\alpha(\mathbf{x}) = \arg \min_y \{y : \hat{F}(y|X = \mathbf{x}) \geq \alpha\}. \quad (10)$$

### C. Prediction interval

The QRF model can be used to construct prediction intervals. For example, an 85% prediction interval for the output  $Y$  is estimated by

$$\hat{I}(\mathbf{x}) = [\hat{Q}_{0.075}(\mathbf{x}), \hat{Q}_{0.925}(\mathbf{x})], \quad (11)$$

which should be interpreted as; given  $X = \mathbf{x}$ , a new observation of output  $Y$  is in the interval  $\hat{I}(\mathbf{x})$  with a probability of 85%. The length of the prediction intervals  $\hat{I}(\mathbf{x})$  reflects the reliability of the predictions.

### D. Permutation importance

In order to understand the underlying battery degradation process, the goal of battery cycle life prediction should not only be limited to learn a regression function  $\hat{f}$  that is capable of making battery cycle life predictions with high accuracy, but also to identify input variables from feature engineering that are the most important for the prediction accuracy of the learned model. A tool like variable importance can be helpful for identifying which input variables that are the most important and therefore should be measured with high precision [37].

The concept of variable importance was first introduced by Breiman for random forests, in which variable importance of an input variable is measured by the decrease in prediction accuracy when the values of this input variable are randomly permuted/shuffled in out-of-bag samples and then dropping the out-of-bag samples down the corresponding trees. [36]. Louppe et al. [38] characterized an alternative measure of variable importance based on the Mean Decrease Impurity (MDI). Impurity is quantified by the splitting criterion of the decision trees (e.g., mean squared error for continuous outputs). However, variable importance based on MDI method favors high cardinality input variables over low cardinality input variables, such as binary variables or categorical variables with a small number of possible categories. Furthermore, variable importance based on MDI method can only be calculated on training set during growth of trees. Therefore, there are possibilities that MDI method gives high importance to input variables that may not be predictive on unseen data when the model is overfitted [38]. With the aim of mitigating those limitations of variable importance based on MDI method, permutation importance is developed as a generalized model-agnostic method for measuring the importance of an input variable by calculating the increase of prediction error after permuting values of the input variable [37]. An input variable is considered to be important if shuffling its value leads to an increase of the model error and vice versa. Permutation importance can be computed on both the training set and the test set, which makes it possible to identify features that contribute the most to the generalized prediction power of the fitted model. Input variables that are important on the training set but not on the test set might make the model overfit. The permutation importance algorithm below describes how the measure is calculated.

### E. Partial dependence plot

After the most important input variables have been identified, the following step is to understand the dependence of the approximation  $\hat{f}(X)$  on the joint values of the input variables [39].

Consider the subvector  $X_S$  of  $\ell < p$  of the input vector  $X = (X_1, X_2, \dots, X_p)^T$ , indexed by  $S \subset \{1, 2, \dots, p\}$ . Let  $\mathcal{C}$  be the complement set, with  $S \cup \mathcal{C} = \{1, 2, \dots, p\}$ . The approximation  $\hat{f}(X)$  in principle depends on all of the input variables  $\hat{f}(X) = \hat{f}(X_S, X_{\mathcal{C}})$ . If the variables in  $X_S$  do not

---

**Algorithm 1** The permutation importance algorithm
 

---

- 1: **Input:** Learned model  $\hat{f}$ , training or test set  $\mathcal{G}$ , and error score function  $s$  (e.g.,  $R^2$  score)
  - 2: Compute the reference error score  $s_0$  of the learned model  $\hat{f}$  on data set  $\mathcal{G}$
  - 3: **for** each input variable  $j = 1, 2, \dots, p$  **do**
  - 4:   **for** each repetition  $m = 1, 2, \dots, M$  **do**
  - 5:     Randomly shuffle the values in the column of input variable  $j$  in data set  $\mathcal{G}$  to generate a corrupted version of the data set  $\tilde{\mathcal{G}}$
  - 6:     Compute the error score  $s_{j,m}$  of the learned model  $\hat{f}$  on corrupted version of the data set  $\tilde{\mathcal{G}}$
  - 7:   **end for**
  - 8:   Compute importance  $\text{Im}_j$  for input variable  $j$  defined as  $\text{Im}_j = s_0 - \frac{1}{M} \sum_{m=1}^M s_{j,m}$
  - 9: **end for**
  - 10: Sort input variables in descending order of variable importance.
- 

have strong interactions with those in  $X_C$ , then the average or partial dependence of  $\hat{f}(X)$  on  $X_S$  is

$$\hat{f}_S(X_S) = E_{X_C}[\hat{f}(X)] = E_{X_C}[\hat{f}(X_C, X_S)]. \quad (12)$$

In practice, the partial dependence function  $\hat{f}_S(X_S)$  can be estimated by

$$\bar{f}_S(X_S) = \frac{1}{N} \sum_{i=1}^N \hat{f}(X_S, \mathbf{x}_{iC}), \quad (13)$$

where  $\{\mathbf{x}_{1C}, \mathbf{x}_{2C}, \dots, \mathbf{x}_{NC}\}$  are the values of  $X_C$  occurring in the training set, and  $N$  is the total number of samples in the training set.

#### IV. EXPERIMENTAL VALIDATION

##### A. Battery dataset

The battery dataset used in the present work is originally from the work of Toyota Research Institute in collaboration with Stanford University and MIT [5]. An early-prediction model developed in their work [5] was later used for selecting high-cycle-life charging protocols [6]. There are 124 lithium iron ferrous phosphate (LFP)/graphite cells in this dataset with a nominal capacity of 1.1 Ah. The total 124 cells are from 3 batches (i.e., the "2017-05-12" batch, the "2017-06-30" batch, and the "2018-04-12" batch) with batch date referring to the date the batch started. The cells are charged with a one-step or two-step fast-charging protocol and discharged at 4 C-rate. It is assumed that the lithium-ion batteries reach their end of life (EOL) when their discharge capacity has decreased to 80% of their initial nominal capacity.

##### B. Train-test split

The dataset was randomly divided into a training set (i.e., 27 cells from the "2017-05-12" batch, 36 cells from the "2017-06-30" batch, and 36 cells from the "2018-04-12" batch) and a test set (i.e., 14 cells from the "2017-05-12" batch, 7 cells from the "2017-06-30" batch, and 4 cells from the "2018-04-12" batch).

##### C. Performance evaluation metrics

1) *Evaluating point prediction accuracy:* There are various performance evaluation metrics that can be used to evaluate the accuracy of point predictions. The most common ones are coefficient of determination ( $R^2$ ), root mean squared error (RMSE), and mean absolute percentage errors (MAPE). They are defined as follows:

$$R^2(y_i, \hat{y}_i) = 1 - \frac{\sum_{i=1}^{N_T} (y_i - \hat{y}_i)^2}{\sum_{i=1}^{N_T} (y_i - \bar{y})^2} \quad (14)$$

$$\text{RMSE}(y_i, \hat{y}_i) = \sqrt{\frac{1}{N_T} \sum_{i=1}^{N_T} (y_i - \hat{y}_i)^2} \quad (15)$$

$$\text{MAPE}(y_i, \hat{y}_i) = \frac{1}{N_T} \sum_{i=1}^{N_T} \left| \frac{y_i - \hat{y}_i}{y_i} \right| \quad (16)$$

where  $N_T$  is the number of samples to be evaluated (i.e., all samples in the test set),  $\hat{y}_i = \hat{f}(\mathbf{x}_i)$  denotes the estimated mean cycle life predicted by the model, and  $y_i$  denotes the corresponding observed cycle life. The average cycle life is  $\bar{y} = \frac{1}{N_T} \sum_{i=1}^{N_T} y_i$  for a total of  $N_T$  samples in the test set.

2) *Evaluating range prediction and calibration error:* The prediction interval coverage probability (PICP) is employed to evaluate the accuracy of prediction intervals. The PICP shows the percentage of output values to be covered by the lower and upper bounds of the prediction intervals. A larger PICP means that more output values will fall in the constructed prediction intervals, and vice versa. The PICP is defined as [40],

$$\text{PICP} = \frac{1}{N} \sum_{i=1}^N c_i, \quad (17)$$

where  $c_i$  is a binary variable that only takes two values, either 0 or 1. If the output value  $y_i$  is covered by the interval from the lower bound  $L_i$  to the upper bound  $U_i$  of the constructed prediction interval, then  $c_i = 1$ ; otherwise  $c_i = 0$ . Ideally, the PICP should be as close to its nominal value as possible, which in reality does not happen very often, unfortunately.

It is common practice to choose the nominal coverage probabilities for prediction intervals by convention, and then compare the actual coverage probabilities with the nominal coverage probabilities in order to assess the performance of the quantile regression models [41] [42]. In these work, only a limited number of nominal coverage probabilities are selected and assessed. Here, we propose an area-based error score (ABES) function for tuning hyperparameters of the QRF model so as to calibrate coverage probabilities associated with prediction intervals, and also for subsequent assessment of calibration error on test set. The prediction interval coverage probability vs. its corresponding actual coverage probability is plotted and then the resulting curve is compared with the reference line, as visualized in Fig. 4. The ABES is then calculated as

$$\text{ABES} = \frac{A}{B} \times 100\%, \quad (18)$$

where  $A$  denotes area enclosed by the curve of actual coverage probability vs. prediction interval coverage probability (in red

color) and reference line (in black color) and shaded with red color, and  $B$  denotes the area of the lower triangle under reference line shaded with grey color (see Fig. 4).

#### D. Expected battery cycle life of a charging protocol

In an application of selecting the high-cycle-life charging protocol, the expected battery cycle life of a charging protocol can be calculated in different ways. In the case where only point predictions are available, the expected battery cycle life can be calculated by averaging over all predicted mean cycle lives of cells charged with this charging protocol,

$$\text{ECL}_1 = \frac{1}{B} \sum_{i=1}^B \hat{f}(\mathbf{x}_i), \quad (19)$$

where  $B$  denotes the total number of battery cells charged with this charging protocol.

In the case where both point prediction and range prediction are available, the expected cycle life of a charging protocol can be calculated as a weighted sum over all predicted mean cycle lives with the weight inversely proportional to the length of prediction intervals,

$$\text{ECL}_2 = \sum_{i=1}^B v_i \hat{f}(\mathbf{x}_i), \quad (20)$$

where  $v_i$  is the weight that is defined as

$$v_i = \frac{\frac{1}{U_i - L_i}}{\sum_{i=1}^B \frac{1}{U_i - L_i}}, \quad (21)$$

with the sum of all weights equal to 1. The length of a constructed prediction interval is the upper bound  $U_i$  minus the lower bound  $L_i$ .

## V. PERFORMANCE EVALUATION AND APPLICATION CASES

### A. Point prediction of battery cycle life

The QRF model is capable of providing point predictions (i.e., predicted mean of cycle life). The accuracy of point prediction of the QRF model is compared with that of Elastic Net regression model [5]. For a fair comparison, both QRF model and Elastic Net model are trained on the same training set, their averaged performance given a set of hyperparameters is evaluated via the same LOO-XVE, and their hyperparameters are tuned for the same number of trails (i.e., 250 times) via Optuna. The point prediction accuracy of two final models is evaluated on the same test set with three performance evaluation metrics. The results are shown in Fig. 2.

As illustrated in Fig. 2, the black diagonal lines show "perfect" predictions, i.e., when the predicted mean of battery cycle life is exactly the same as the observed battery cycle life. In terms of point prediction accuracy, the point prediction of battery cycle life by QRF is found to outperform Elastic Net regression model, evaluated by all three performance measures, i.e.,  $R^2$ , RMSE, and MAPE.

Fig. 3 shows a sensitivity analysis of the QRF model and Elastic Net regression model performance using different number of early-cycle data (from first 25 cycles to first 250

cycles). Ten different models of each were then learned from ten different training sets extracted from ten different number of early cycles data, and then evaluated w.r.t. RMSE and MAPE on the test set. It can be seen in Fig. 3a that initially, the prediction errors significantly decrease with increasing number of early-cycle data used. However, after 125 cycles, the prediction errors start to increase again. For the Elastic Net regression model (see Fig. 3b), the lowest prediction errors are also obtained at 125 cycles, but with values higher than that of the QRF model. However, each charge-discharge cycle takes 50 min on average, and consequently, 25 cycles translates to around 21 hours, which brings more experimental time and costs. Using the first 100 cycles could be a suitable trade-off between prediction accuracy and required number of cycles. The reason why the prediction error varies over the number of early cycles used is because predictive power of extracted features varies with the number of cycles. It can be concluded that given the same feature engineering, the non-parametric QRF model is capable of providing better battery cycle life prediction accuracy than parametric Elastic Net model.

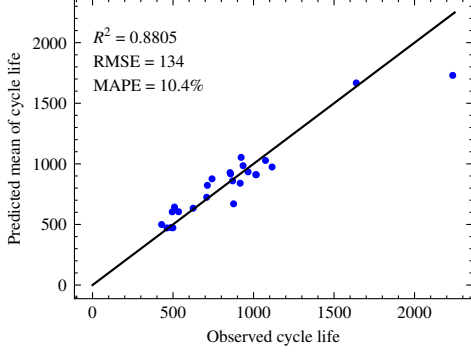
### B. Range prediction of battery cycle life range

For tuning the hyperparameters of the QRF model at the training and cross-validation stages and assessing the accuracy of prediction intervals over all nominal coverage probabilities, the area-based performance evaluation metric ABES (see Eqn. (18)) is used. During the process of tuning hyperparameters of the QRF model, the hyperparameters that result in the lowest ABES score is stored as the optimal set. Then, the QRF model with the optimal hyperparameters is refitted with the entire training set in order to learn the final QRF model. At the test stage, the ABES score and the actual coverage probability for each PICP is calculated on test set. The actual coverage probability vs. PICP is plotted in Fig. 4, yielding an area-based error score of 5.75%.

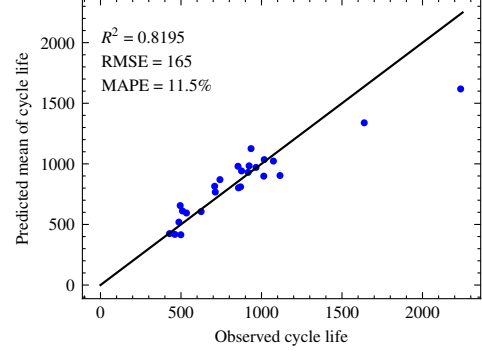
### C. Uncertainty quantification and applications

Based on predicted quantiles, prediction intervals of battery cycle life can be constructed. To examine the prediction performance of the final QRF model in a more intuitive way, we show in Fig. 5 the 85% prediction intervals and the mean predictions made by QRF on the test set. There are 21 out of 25 observed cycle life samples within the prediction intervals resulting in 84% PICP, close to nominal coverage probability 85%, which agrees with the result in Fig. 4. This indicates that the constructed prediction intervals with 85% coverage probability exhibits good coverage probability of the observed cycle life values, which is required for a reliable battery cycle life range prediction.

The upper bound of the 85% prediction interval is the 92.5% quantile prediction of cycle life, which means that battery cycle life may exceed the upper bound with a probability of around 7.5%. Similarly, the lower bound of the 85% prediction interval is the 7.5% quantile prediction of battery cycle life, which means that battery cycle life may exceed the lower bound with a probability of around 92.5%. The lower bound of the prediction intervals would be a conservative decision

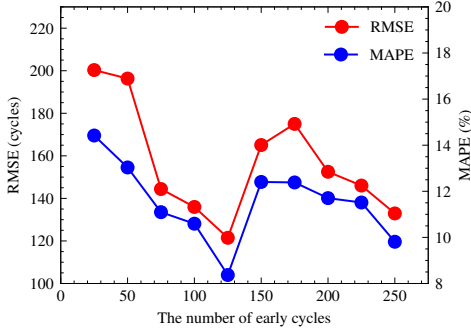


(a) Predicted mean of battery cycle life by QRF

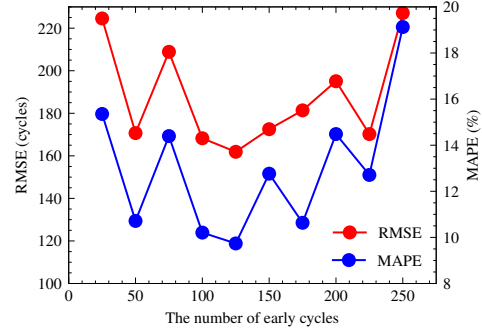


(b) Predicted mean of battery cycle life by Elastic Net

Fig. 2. Observed and predicted cycle life by QRF and Elastic Net respectively.



(a) RMSE and MAPE of battery cycle life prediction by the QRF model.



(b) RMSE and MAPE of battery cycle life prediction by the Elastic Net model.

Fig. 3. RMSE and MAPE of battery cycle life prediction as a function of the number of early cycles used to make predictions.

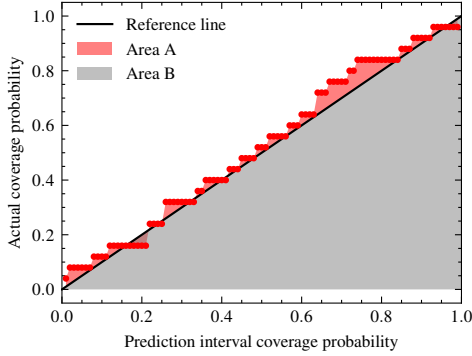


Fig. 4. Prediction interval coverage probability vs. actual coverage probability curve computed on the test set.

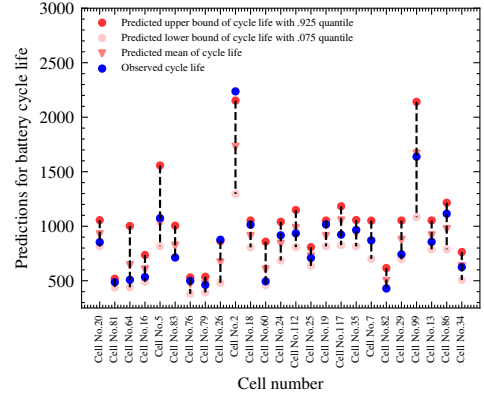


Fig. 5. The 85% prediction intervals and mean predictions by QRF.

while the upper bound would be an optimistic decision. Which decision out of the two that is preferred depends on the specific application scenario. For example, a conservative decision is usually preferred for the battery warranty service offered by automotive companies.

In comparison with point predictions without information about the possible uncertainty in cycle life prediction of any given cell, prediction intervals provide a predicted range cycle life for a given probability. The reliability of a range prediction can thus be assessed by the length of the prediction interval.

The shorter the prediction interval, the more reliable the prediction is. Cells in the test set with a length of prediction interval exceeding a certain threshold (e.g. 350 cycles) are of our particular interest and their cycle life predictions are flagged anomalous. Their values of the most important feature (i.e., variance of  $\Delta Q_{100-10}(V)$ ) are indicated by red dashed lines in the PDP for the cycle life prediction w.r.t. variance of  $\Delta Q_{100-10}(V)$  (see Fig. 6). Two cells to the left in the figure can be explained by lack of observations in that zone.



Interestingly, the values of the variance of  $\Delta Q_{100-10}(V)$  of the remaining four cells fall in two "transition zones", where cycle life decreases dramatically with increasing variance of  $\Delta Q_{100-10}(V)$ . A possible explanation for dramatic changes within two "transition zones" may be the lack of adequate observations between two "transition zones". However, the causal interpretation of the length of prediction intervals is difficult given a small battery dataset in the present work, therefore, may require larger battery dataset and further experimental investigations, for instance, post-mortem analysis. In practice, anomalous predictions of cycle life are not of favor since they do not provide much information for facilitating decision-making.

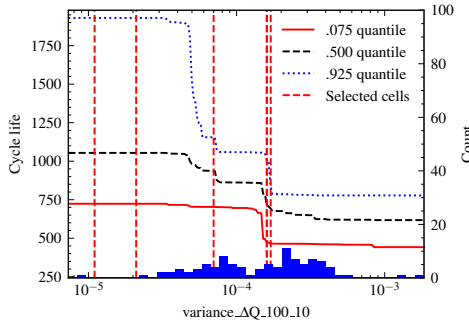


Fig. 6. Selected 6 cells in the test set with a length of prediction interval exceeding 350 cycles. Note that there are 2 cells whose values of variance of  $\Delta Q_{100-10}(V)$  overlap.

For the purpose of demonstrating how the learned QRF model facilitates dual-criteria decision-making to select the high-cycle-life charging protocol which maximizes the expected battery cycle life, two pairs of cells are found in the test set, each pair containing 2 cells from the same batch date and charged with the same charging protocols. The first pair of cells are cell No.18 and cell No.19. Both of them charged with a charging protocol "5.4C(70%)-3C". The difference of predicted mean cycle life between the two cells are 27 cycles, with 947 cycles for cell No.18 and 920 cycles for cell No.19. Moreover, both cells have similar length of prediction intervals (246 cycles for cell No.18, and 236 cycles for cell No.19). The expected battery cycle life of the charging protocol "5.4C(70%)-3C" calculated using Eqn. (19) is equal to 933.5 cycles, while the expected battery cycle life calculated using Eqn. (20) is equal to 933.8 cycles. In fact, the two cells exhibit very similar capacity degradation curve as shown in Fig. 7a. The second pair of cells are cell No.24 and cell No.25. Both of them charged with a charging protocol "6C(40%)-3C". The difference of predicted mean cycle life between the two cells (i.e., 843 cycles for cell No.24 and 729 cycles for cell No.25) are considerably large and equal to 114 cycles. Also, the prediction interval of cell No.24 is much wider than that of cell No.25, suggesting a possible larger discrepancy between predicted mean cycle life and the observed cycle life of cell No.24. The expected battery cycle life of the charging protocol "6C(40%)-3C" calculated using Eqn. (19) is equal to 786 cycles, while the expected battery cycle life calculated using Eqn. (20) is equal to 765.5 cycles. In fact, as it is

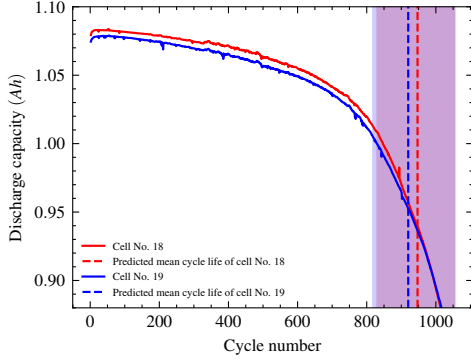
shown in Fig. 7b, the discrepancy between predicted cycle life and the observed cycle life of cell No.24 is much larger than that of cell No.25. The decision based on the two methods of determining expected battery cycle life of a charging protocol is consistent, i.e., the first charging protocol, "5.4C(70%)-3C", is selected.

Based on the two examples given above, it can be concluded that the observed discrepancy between predicted mean cycle life and the observed cycle life of a cell agrees with the length of the prediction interval. The lengths of the prediction intervals may provide more information for decision-making under uncertainties than we get from point predictions alone, for instance, when selecting high-cycle-life charging protocol. Interestingly, the differences in observed cycle life within each pair can be quite remarkable (see Fig. 7b), considering that they are expected to have almost the same aging process. The reason why cells from the same batch and charged with the same charging protocols can have a very different cycle life is most likely due to production-related factors (e.g., the variance of material properties and process parameters). Apparently, in this case, the cell-to-cell variations caused by the production process are quite significant, and these variations are indeed captured by the model via the extracted features.

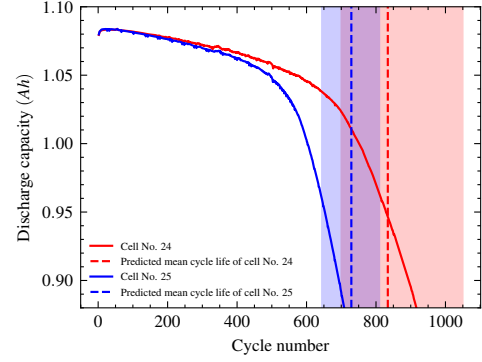
## VI. MODEL INTERPRETATION

Permutation importance is computed on the training set as shown in Fig. 8a. The two most important features identified are related to the  $\Delta Q_{100-10}(V)$  curve, i.e., the discharge capacity change as a function of voltage between cycle 100 and cycle 10, which was selected in the cycle life prediction model developed by Kristen et al. [5]. This  $\Delta Q(V)$  curve is of great interest because the curve itself and its derivatives contain rich information for degradation diagnosis [43] [44] [45]. Based on the training set, the most important feature is the variance of  $\Delta Q_{100-10}(V)$  curve (see [5] for the definition of this feature), which means that the QRF model relies on this feature the most for making predictions. However, measuring the feature importance on the training set on which the QRF model is trained is not as informative as that on the unseen data. If the QRF model is overfitted, the feature importance measured on the training set may mislead us to believe that the wrong features are important. Therefore, the feature importance is also measured on the test set. It is shown in Fig. 8b that the most importance feature is still the variance of  $\Delta Q_{100-10}(V)$  curve, which means that this feature does indeed contribute the most to the prediction performance of the QRF model.

In order to further illustrate how the most important feature affects the predicted cycle life, a one dimensional partial dependence plot (PDP) is computed on the training set and is illustrated in Fig. 9. A lower bound of the predicted battery cycle life as a function of variance of  $\Delta Q_{100-10}(V)$  is provided by the .075 quantile curves, while the .925 quantile curve provides an upper bound of the predicted battery cycle life as a function of variance of  $\Delta Q_{100-10}(V)$ . The median value of the predicted battery cycle life is provided by the .50 quantile curves. The histogram on the x-axis

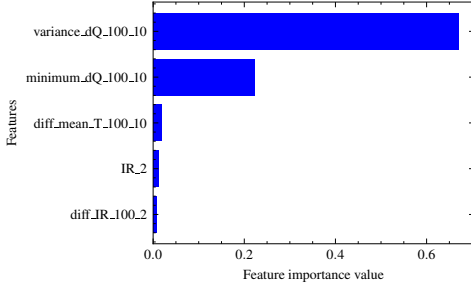


(a) Predicted mean and 85% prediction interval of Cell No.18 and Cell No.19

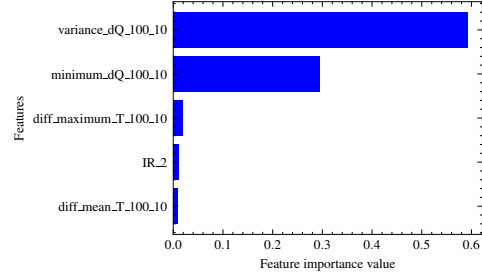


(b) Predicted mean and 85% prediction interval of Cell No.24 and Cell No.25

Fig. 7. Selected two pairs of cells with less than 5 cycle mean predictions.



(a) Training set



(b) Test set

Fig. 8. Permutation importance ranking of top 5 features on training and test set respectively.

shows the distribution of the observations of the variance of  $\Delta Q_{100-10}(V)$  in the training set. The quantile curves flatten out in the region of sparse observations of the variance of  $\Delta Q_{100-10}(V)$  in the training data, which do not provide much information. In the region of dense distribution of variance of  $\Delta Q_{100-10}(V)$  in training set, battery cycle life rapidly decreases when the variance of  $\Delta Q_{100-10}(V)$  increases from  $10^{-10}$  to  $10^{-8}$ , which indicates that a small increase of variance of  $\Delta Q_{100-10}(V)$  during discharge stage has a large effect on battery degradation rate. The physical meaning of the variance of  $\Delta Q_{100-10}(V)$  is associated with the dependence of discharge energy dissipation on voltage. The variance of  $\Delta Q_{100-10}(V)$  reflects the degree of non-uniformity in the discharge energy dissipation with voltage [5]. Thus, the larger value of the variance of  $\Delta Q_{100-10}(V)$  indicates a larger degree of non-uniformity in the discharge energy dissipation under galvanostatic conditions, which is consistent with the monotonic relationship between the variance of  $\Delta Q_{100-10}(V)$  and cycle life (Fig. 9a). The second most importance feature is the minimum of  $\Delta Q_{100-10}(V)$ , for which battery cycle life decreases with increasing value of the minimum of  $\Delta Q_{100-10}(V)$ , but not to the same extent as for the variance of  $\Delta Q_{100-10}(V)$ .

The prediction intervals on both ends (i.e., left and right) of the x-axis are larger than those in the middle of the x-axis. The reason is that observations are lacking on both ends of the x-axis, therefore, the learned QRF model is not confident

to make predictions on these two zones, which leads to larger prediction uncertainty represented by the length of prediction intervals.

Furthermore, we would like to point out that data uncertainties are not considered in the present work, and it is assumed that all measurements are accurate and taken as if they are true.

The PDP results further illustrate how the variance of  $\Delta Q_{100-10}(V)$  and the minimum of  $\Delta Q_{100-10}(V)$  affect the predictions of battery cycle life quantitatively. Similarly, PDPs can be computed for all other features used as inputs to the QRF model on the training set.

Kristen et al. [5] rationalized highly predictive features extracted from early-cycle discharge voltage curves (i.e., the variance of  $\Delta Q_{100-10}(V)$  and the minimum of  $\Delta Q_{100-10}(V)$ ) by investigating degradation modes that do not lead to immediate capacity fade but are manifested in the discharge voltage curves. They concluded that loss of active material of the delithiated negative electrode contributes to a shift in the discharge voltage curve, with no change in capacity fade, as is the case of commercial LFP/graphite cells operating under similar conditions. At high number of cycles, loss of active material of the delithiated negative electrode induces lithium plating, which irreversibly accelerates capacity loss. Additional experiments were conducted by Kristen et al. [5] to quantitatively investigate the contribution of loss of active material of the delithiated negative electrode to shifts in

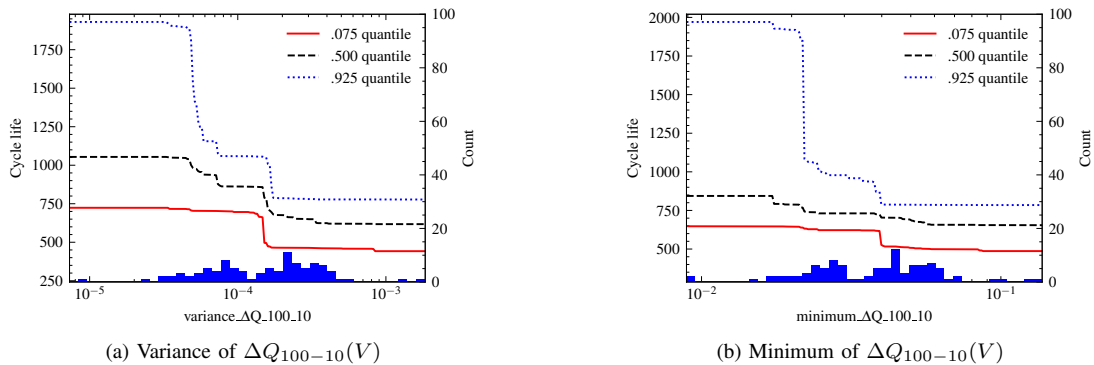


Fig. 9. PDPs for the cycle life prediction w.r.t. variance of  $\Delta Q_{100-10}(V)$  and minimum of  $\Delta Q_{100-10}(V)$ . Histogram at the bottom shows observations of the feature, with scale to the right.

$dQ/dV$  and  $dV/dQ$  observed in diagnostic cycling. It was found that loss of active material of the delithiated negative electrode alters a fraction of the discharge voltage curve which is consistent with the high feature importance of variance and minimum of  $\Delta Q(V)$ , as shown in Fig. 8.

## VII. CONCLUSION

In the present paper, we have proposed a QRF model for Li-ion battery cycle life prediction using early degradation data. Compared to previous work by other researchers, the QRF model is capable of not only providing point prediction with high accuracy, but also battery cycle life range prediction with uncertainty quantified as the length of prediction intervals, which can be crucial for Li-ion battery applications. The final QRF model was produced from a machine learning pipeline on a public battery dataset. In total 33 features were extracted from the early cycles. A novel area-based performance evaluation metric has been proposed for tuning hyperparameters of the QRF model when applying it for prediction intervals. The final QRF model was interpreted using two global model-agnostic methods - permutation importance and one dimensional PDP. With permutation importance ranking method, the features that contribute the most to the prediction results were identified. To further illustrate how these most important features affect the predicted cycle life, one-dimensional PDP was computed to quantitatively visualize how features affect battery cycle life where upper and lower bound of battery cycle life were provided. Comparing with Elastic Net regression model, the QRF model provides competitive point prediction accuracy. Moreover, prediction intervals were constructed based on the QRF model which can be extremely useful especially when point predictions of cycle life are close to each other. Two examples were given to show that prediction intervals can contribute to better multi-criteria decision-making in sensitive cases, for example, when selecting the charging protocol that results in as long expected battery cycle life as possible.

To the best of our knowledge, it is first time that the QRF model is introduced to battery cycle life range prediction even though it has been used in predictions of drug effect, crop yield etc. Two global model-agnostic methods were employed to interpret the final QRF model, and they can be easily

employed also for other advanced data-driven methods. These interpretable techniques can reveal underlying battery aging mechanisms and help finding features that have the most predictive power for cycle life prediction with data-driven methods. There are, however, several improvements to be made in future work. First, the dataset used for training and testing is relatively small in contrast to the size of datasets commonly used for training QRF model, such as in crop yield predictions. A larger dataset is desired for validating prediction performance of the QRF model and revealing a better picture of the battery degradation process. Second, permutation importance and PDP are the two methods used in the present work to implicitly interpret the model. Additional interpretable techniques can be introduced in the future for further interpretation of other advanced data-driven model. Third, the battery calendar aging effect due to storage is not considered in this work, which could be taken into account in the future model if storage conditions are known. Finally, with uncertainty level of predictions quantified as length of prediction intervals, a natural next step would be to find out what contributes to the length of prediction intervals so that charging protocols that cause high uncertainty associated with cycle life prediction can be avoided.

## ACKNOWLEDGMENT

The authors would like to thank Volvo AB and Swedish Energy Agency for funding this work.

## REFERENCES

- [1] M. A. Hannan, M. H. Lipu, A. Hussain, and A. Mohamed, "A review of lithium-ion battery state of charge estimation and management system in electric vehicle applications: Challenges and recommendations," *Renewable and Sustainable Energy Reviews*, vol. 78, pp. 834–854, 2017.
- [2] G. Zubi, R. Dufo-López, M. Carvalho, and G. Pasaoglu, "The lithium-ion battery: State of the art and future perspectives," *Renewable and Sustainable Energy Reviews*, vol. 89, pp. 292–308, 2018.
- [3] J. Vetter, P. Novák, M. R. Wagner, C. Veit, K.-C. Möller, J. Besenhard, M. Winter, M. Wohlfahrt-Mehrens, C. Vogler, and A. Hammouche, "Ageing mechanisms in lithium-ion batteries," *Journal of power sources*, vol. 147, no. 1-2, pp. 269–281, 2005.
- [4] E. Martinez-Laserna, I. Gandiaga, E. Sarasketa-Zabala, J. Badeda, D.-I. Stroe, M. Swierczynski, and A. Goikoetxea, "Battery second life: Hype, hope or reality? a critical review of the state of the art," *Renewable and Sustainable Energy Reviews*, vol. 93, pp. 701–718, 2018.

- [5] K. A. Severson, P. M. Attia, N. Jin, N. Perkins, B. Jiang, Z. Yang, M. H. Chen, M. Aykol, P. K. Herring, D. Fraggedakis *et al.*, "Data-driven prediction of battery cycle life before capacity degradation," *Nature Energy*, vol. 4, no. 5, pp. 383–391, 2019.
- [6] P. M. Attia, A. Grover, N. Jin, K. A. Severson, T. M. Markov, Y.-H. Liao, M. H. Chen, B. Cheong, N. Perkins, Z. Yang *et al.*, "Closed-loop optimization of fast-charging protocols for batteries with machine learning," *Nature*, vol. 578, no. 7795, pp. 397–402, 2020.
- [7] P. Fermín-Cueto, E. McTurk, M. Allerhand, E. Medina-Lopez, M. F. Anjos, J. Sylvester, and G. Dos Reis, "Identification and machine learning prediction of knee-point and knee-onset in capacity degradation curves of lithium-ion cells," *Energy and AI*, vol. 1, p. 100006, 2020.
- [8] T. Baumhöfer, M. Brühl, S. Rothgang, and D. U. Sauer, "Production caused variation in capacity aging trend and correlation to initial cell performance," *Journal of Power Sources*, vol. 247, pp. 332–338, 2014.
- [9] M. Huang, M. Kumar, C. Yang, and A. Soderlund, "Aging estimation of lithium-ion battery cell using an electrochemical model-based extended kalman filter," in *AIAA Scitech 2019 Forum*, 2019, p. 0785.
- [10] C. Lyu, Q. Lai, T. Ge, H. Yu, L. Wang, and N. Ma, "A lead-acid battery's remaining useful life prediction by using electrochemical model in the particle filtering framework," *Energy*, vol. 120, pp. 975–984, 2017.
- [11] Y. Chang, H. Fang, and Y. Zhang, "A new hybrid method for the prediction of the remaining useful life of a lithium-ion battery," *Applied energy*, vol. 206, pp. 1564–1578, 2017.
- [12] L. Zhang, Z. Mu, and C. Sun, "Remaining useful life prediction for lithium-ion batteries based on exponential model and particle filter," *IEEE Access*, vol. 6, pp. 17 729–17 740, 2018.
- [13] E. Sarasketa-Zabala, E. Martinez-Laserna, M. Berecibar, I. Gandiaga, L. M. Rodriguez-Martinez, and I. Villarreal, "Realistic lifetime prediction approach for li-ion batteries," *Applied energy*, vol. 162, pp. 839–852, 2016.
- [14] M. Schimpe, M. E. von Kuepach, M. Naumann, H. C. Hesse, K. Smith, and A. Jossen, "Comprehensive modeling of temperature-dependent degradation mechanisms in lithium iron phosphate batteries," *Journal of The Electrochemical Society*, vol. 165, no. 2, p. A181, 2018.
- [15] J. de Hoog, J.-M. Timmermans, D. Ioan-Stroe, M. Swierczynski, J. Jaguemont, S. Goutam, N. Omar, J. Van Mierlo, and P. Van Den Bossche, "Combined cycling and calendar capacity fade modeling of a nickel-manganese-cobalt oxide cell with real-life profile validation," *Applied Energy*, vol. 200, pp. 47–61, 2017.
- [16] B. Long, W. Xian, L. Jiang, and Z. Liu, "An improved autoregressive model by particle swarm optimization for prognostics of lithium-ion batteries," *Microelectronics Reliability*, vol. 53, no. 6, pp. 821–831, 2013.
- [17] Y. Zhou and M. Huang, "Lithium-ion batteries remaining useful life prediction based on a mixture of empirical mode decomposition and arima model," *Microelectronics Reliability*, vol. 65, pp. 265–273, 2016.
- [18] J. Wu, C. Zhang, and Z. Chen, "An online method for lithium-ion battery remaining useful life estimation using importance sampling and neural networks," *Applied energy*, vol. 173, pp. 134–140, 2016.
- [19] X. Hu, S. E. Li, and Y. Yang, "Advanced machine learning approach for lithium-ion battery state estimation in electric vehicles," *IEEE Transactions on Transportation Electrification*, vol. 2, no. 2, pp. 140–149, 2015.
- [20] Y. Zhang, R. Xiong, H. He, and M. G. Pecht, "Long short-term memory recurrent neural network for remaining useful life prediction of lithium-ion batteries," *IEEE Transactions on Vehicular Technology*, vol. 67, no. 7, pp. 5695–5705, 2018.
- [21] A. Nuhic, T. Terzimehic, T. Soczka-Guth, M. Buchholz, and K. Dietmayer, "Health diagnosis and remaining useful life prognostics of lithium-ion batteries using data-driven methods," *Journal of power sources*, vol. 239, pp. 680–688, 2013.
- [22] T. Qin, S. Zeng, and J. Guo, "Robust prognostics for state of health estimation of lithium-ion batteries based on an improved pso-svr model," *Microelectronics Reliability*, vol. 55, no. 9-10, pp. 1280–1284, 2015.
- [23] M. Kläs and A. M. Vollmer, "Uncertainty in machine learning applications: A practice-driven classification of uncertainty," in *International Conference on Computer Safety, Reliability, and Security*. Springer, 2018, pp. 431–438.
- [24] R. R. Richardson, M. A. Osborne, and D. A. Howey, "Battery health prediction under generalized conditions using a gaussian process transition model," *Journal of Energy Storage*, vol. 23, pp. 320–328, 2019.
- [25] D. Liu, J. Pang, J. Zhou, Y. Peng, and M. Pecht, "Prognostics for state of health estimation of lithium-ion batteries based on combination gaussian process functional regression," *Microelectronics Reliability*, vol. 53, no. 6, pp. 832–839, 2013.
- [26] D. Wang, Q. Miao, and M. Pecht, "Prognostics of lithium-ion batteries based on relevance vectors and a conditional three-parameter capacity degradation model," *Journal of Power Sources*, vol. 239, pp. 253–264, 2013.
- [27] D. Liu, J. Zhou, D. Pan, Y. Peng, and X. Peng, "Lithium-ion battery remaining useful life estimation with an optimized relevance vector machine algorithm with incremental learning," *Measurement*, vol. 63, pp. 143–151, 2015.
- [28] R. Koenker and G. Bassett Jr, "Regression quantiles," *Econometrica: journal of the Econometric Society*, pp. 33–50, 1978.
- [29] R. Koenker, "Quantile regression cambridge univ," 2005.
- [30] M. Yousefi-Azar, V. Varadharajan, L. Hamey, and U. Tupakula, "Autoencoder-based feature learning for cyber security applications," in *2017 International joint conference on neural networks (IJCNN)*. IEEE, 2017, pp. 3854–3861.
- [31] X. Bi and H. Wang, "An enhanced high-order boltzmann machine for feature engineering," *Engineering Applications of Artificial Intelligence*, vol. 78, pp. 37–52, 2019.
- [32] P. Guo, Z. Cheng, and L. Yang, "A data-driven remaining capacity estimation approach for lithium-ion batteries based on charging health feature extraction," *Journal of Power Sources*, vol. 412, pp. 442–450, 2019.
- [33] N. Williard, W. He, M. Osterman, and M. Pecht, "Comparative analysis of features for determining state of health in lithium-ion batteries," *International Journal of Prognostics and Health Management*, vol. 4, no. 1, 2013.
- [34] J. H. Friedman, *The elements of statistical learning: Data mining, inference, and prediction*. springer open, 2017.
- [35] T. Akiba, S. Sano, T. Yanase, T. Ohta, and M. Koyama, "Optuna: A next-generation hyperparameter optimization framework," in *Proceedings of the 25th ACM SIGKDD international conference on knowledge discovery & data mining*, 2019, pp. 2623–2631.
- [36] L. Breiman, "Random forests," *Machine learning*, vol. 45, no. 1, pp. 5–32, 2001.
- [37] A. Fisher, C. Rudin, and F. Dominici, "All models are wrong, but many are useful: Learning a variable's importance by studying an entire class of prediction models simultaneously," *J. Mach. Learn. Res.*, vol. 20, no. 177, pp. 1–81, 2019.
- [38] G. Louppe, L. Wehenkel, A. Suter, and P. Geurts, "Understanding variable importances in forests of randomized trees," *Advances in neural information processing systems*, vol. 26, pp. 431–439, 2013.
- [39] J. H. Friedman, "Greedy function approximation: a gradient boosting machine," *Annals of statistics*, pp. 1189–1232, 2001.
- [40] A. Khosravi, S. Nahavandi, and D. Creighton, "Construction of optimal prediction intervals for load forecasting problems," *IEEE Transactions on Power Systems*, vol. 25, no. 3, pp. 1496–1503, 2010.
- [41] H. Wang, "Coverage probability of prediction intervals for discrete random variables," *Computational statistics & data analysis*, vol. 53, no. 1, pp. 17–26, 2008.
- [42] J. Landon and N. D. Singpurwalla, "Choosing a coverage probability for prediction intervals," *The American Statistician*, vol. 62, no. 2, pp. 120–124, 2008.
- [43] I. Bloom, L. K. Walker, J. K. Basco, D. P. Abraham, J. P. Christophersen, and C. D. Ho, "Differential voltage analyses of high-power lithium-ion cells. 4. cells containing nmc," *Journal of Power Sources*, vol. 195, no. 3, pp. 877–882, 2010.
- [44] C. R. Birkel, M. R. Roberts, E. McTurk, P. G. Bruce, and D. A. Howey, "Degradation diagnostics for lithium ion cells," *Journal of Power Sources*, vol. 341, pp. 373–386, 2017.
- [45] M. Berecibar, F. Devriendt, M. Dubarry, I. Villarreal, N. Omar, W. Verbeke, and J. Van Mierlo, "Online state of health estimation on nmc cells based on predictive analytics," *Journal of Power Sources*, vol. 320, pp. 239–250, 2016.